Imaging and 3D Elemental Characterization of Intact Bacterial Spores by High-Resolution Secondary Ion Mass Spectrometry

ARTICLE *in* ANALYTICAL CHEMISTRY · JULY 2008

Impact Factor: 5.64 · DOI: 10.1021/ac8006279 · Source: PubMed

7 AUTHORS, INCLUDING:

Stewart J. Fallon
Australian National University
109 PUBLICATIONS **3,645** CITATIONS

SEE PROFILE

Ian Hutcheon
Lawrence Livermore National Laboratory
445 PUBLICATIONS **7,950** CITATIONS

SEE PROFILE

Peter Kilian Weber
Lawrence Livermore National Laboratory
148 PUBLICATIONS **3,071** CITATIONS

SEE PROFILE

Anal. Chem. **2008,** *80,* 5986–5992

Imaging and 3D Elemental Characterization of Intact Bacterial Spores by High-Resolution Secondary Ion Mass Spectrometry

Sutapa Ghosal,*,† Stewart J. Fallon,†,‡ Terrance J. Leighton,§ Katherine E. Wheeler,§ Michael J. Kristo,† Ian D. Hutcheon,† and Peter K. Weber†

Lawrence Livermore National Laboratory, Livermore, California 94551, and Children's Hospital Oakland Research Institute, Oakland, California 94609

We present a quantitative, imaging technique based on nanometer-scale secondary ion mass spectrometry for mapping the 3D elemental distribution present in an individual micrometer-sized *Bacillus* spore. We use depth profile analysis to access the 3D compositional information of an intact spore without the additional sample preparation steps (fixation, embedding, and sectioning) typically used to access substructural information in biological samples. The method is designed to ensure sample integrity for forensic characterization of *Bacillus* spores. The minimal sample preparation/alteration required in this methodology helps to preserve sample integrity. Furthermore, the technique affords elemental distribution information at the individual spore level with nanometer-scale spatial resolution and high (μg/g) analytical sensitivity. We use the technique to map the 3D elemental distribution present within *Bacillus thuringiensis israelensis* spores.

In recent years, there has been significant interest in developing new forensic methods for the characterization of biological materials such as *Bacillus* spores.[1–8] Nongenetic identifiers such as elemental and isotopic signatures provide complementary information that might be useful for ascertaining information about the production of biological agents. There have been a number of studies suggesting that there is a close relationship between the chemical composition of bacterial spores and their source history.[4,6–8] Our laboratory is investigating whether the distribution and abundance of elements at the individual spore level can be used as a forensic tool. The first step toward establishing the forensic potential of elemental distribution in spores is to develop the capability to make accurate measurements at the scale of the spore internal structure. Analysis of individual spores, independent of contaminants or additives, poses a significant challenge because of their small dimensions (~1-μm diameter). Electron microscopy-based X-ray microanalytical techniques[9,10] have been applied to the characterization of individual bacterial spores. These techniques are effective in characterizing major and minor elements (>0.1% by mass) but lack the sensitivity required for trace elemental analysis. Also, they require additional sample preparation steps such as fixation, embedding, and sectioning, which can introduce physical and chemical artifacts. Since preservation of sample integrity is a critical component of forensic methodology, minimizing sample preparation/alteration is desirable. In this paper, we present depth profile analysis using nanometer-scale secondary ion mass spectrometry (NanoSIMS),[11–15] which enables quantitative elemental characterization of single, intact *Bacillus* spore with minimal sample preparation. Using this technique, we have directly mapped the penetration and distribution of Li ions in spores suspended in aqueous lithium fluoride solution.

Depth profile analysis of individual biological cells poses significant challenges.[16] Biological samples are inherently complex, both compositionally and texturally. While previous work on depth-resolved imaging at the scale of eukaryotic cells has been indicative of the expected chemical structure of large subcellular regions, such as the nucleoli,[12,16] to the best our knowledge there have been no studies reported that test this capability in a quantitative and controlled set of experiments using biological samples in the micrometer size range (<10 μm). Bacterial spores provide the ideal template for performing such systematic studies since they are chemically structured in a known, radially symmetric manner and do not contain significant textural irregulari-

* To whom correspondence should be addressed. E-mail: ghosal2@llnl.gov.
† Lawrence Livermore National Laboratory.
‡ Present address: The Australian National University, Canberra, Australia.
§ Children's Hospital Oakland Research Institute.

(1) Westphal, A. J.; Buford Price, P.; Leighton, T. J.; Wheeler, K. E. *Proc. Natl. Acad. Sci. U. S. A.* **2003**, *100*, 3461–3466.
(2) Ryzhov, V.; Hathout, Y.; Fenselau, C. *Appl. Environ. Microbiol.* **2000**, *66*, 3828–3834.
(3) Whiteaker, J. R.; Fenselau, C.; Fetterolf, D.; Steele, D.; Wilson, D. *Anal. Chem.* **2004**, *76*, 2836–2841.
(4) Cliff, J. B.; et al. *Appl. Environ. Microbiol.* **2005**, *71*, 6524–6530.
(5) Gikunju, C. M.; Lev, S. M.; Birenzvige, A.; Schaefer, D. M. *Talanta* **2004**, *62*, 741–744.
(6) Horita, J.; Vass, A. A. *J. Forensics Sci.* **2003**, *48*, 1–5.
(7) Kreuzer-Martin, H. W.; Lott, M. J.; Dorigan, J. V.; Ehleringer, J. R. *Proc. Natl. Acad. Sci. U. S. A.* **2003**, *100*, 815–819.
(8) Kreuzer-Martin, H. W.; Chesson, L. A.; Lott, M. J.; Dorigan, J. V.; Ehleringer, J. R. *J. Forensics Sci.* **2004**, *49*, 1–7.
(9) Stewart, M.; et al. *J. Bacteriol.* **1980**, *143*, 481–491.
(10) Gerhardt, P.; Pankratz, H. S.; Scherrer, R. *Appl. Environ. Microbiol.* **1976**, *32*, 438–440.
(11) Lechene, C. P.; et al. *J. Biol.* **2006**, *5*, 20–30.
(12) McMahon, G.; Glassner, B. J.; Lechene, C. P. *Appl. Surf. Sci.* **2006**, *252*, 6895–6906.
(13) Castaing, R.; Slodzian, G. *J. Microsc.* **1962**, *1*, 31–38.
(14) Kraft, M. L.; et al. *Science* **2006**, *313*, 1948–1951.
(15) Moreau, J. W.; et al. *Science* **2007**, *316*, 1600–1603.
(16) Fletcher, J. S.; Lockyer, N. P.; Vaidyanathan, S.; Vickerman, J. C. *Anal. Chem.* **2007**, *79*, 2199–2206.

10.1021/ac8006279 CCC: $40.75
Published on Web 06/26/2008

ties, such as voids or surface roughness at the scale of eukaryotic cells.

Secondary ion mass spectrometry (SIMS)-based depth profile analysis has been used to characterize elemental distribution in a variety of inorganic and organic samples.[17–19] However, SIMS-based depth profile analysis of an individual biological cell is challenging partly because the imaging of such small dimensions requires a highly focused ion beam. While standard SIMS instruments are capable of high depth resolution (1−2 nm), the lateral resolution possible with these instruments is at best 5 times lower (typical resolution >1000 nm) compared to the lateral resolution possible with NanoSIMS (50 nm with Cs^+ primary beam, 150 nm with O^-). In addition to high lateral resolution, the NanoSIMS instrument has ~10× higher sensitivity at high mass resolving power compared to conventional SIMS instruments (useful yield (see Supporting Information) approaching 5%), which is critical given the small volume sampled during analysis of single biological cells. NanoSIMS is also capable of simultaneous detection of multiple elemental species (5 species with the NanoSIMS 50 instrument). Kraft et al. and Lechene et al. have used this parallel quantitative mass imaging capability to differentiate between nanometer-scale domains in lipid membranes and subcellular components, respectively.[11,12,14]

To investigate the feasibility of depth profile-based characterization of an intact *Bacillus* spore by NanoSIMS, we analyzed individual *Bacillus thuringiensis israelensis* (*Bti*) spores, which are oblate spheroids approximately 2 by 0.9 μm in dimension.[20] *Bti* spores were used as a surrogate for *Bacillus anthracis* spores, which are of particular forensic interest. *Bacillus* spores are composed of a compartmentalized structure consisting of several concentric layers differing in both composition and morphology (Figure 1a).[9,10] The layered structure is associated with characteristic elemental signatures, the most notable of which are the high phosphorus and calcium content of the core. DNA and RNA, both rich in P, are localized in the spore core. Calcium dipicolinate, which protects and stabilizes the spore core, is the source of its high Ca content. The elemental distribution information acquired by depth profile analysis of a whole spore is compared to that obtained from the surface analysis of a sectioned spore. In addition, we looked at the distribution of lithium in spores exposed to aqueous Li ions to demonstrate the impact of environmental exposure on spore elemental distribution. To characterize the depth resolution possible with the NanoSIMS-based depth profile method we analyzed a silicon−carbon multilayer sample of known dimensions.

EXPERIMENTAL SECTION

Spore Samples. *B. thuringiensis* var. *israelensis* (BGSC 4Q1) strain was obtained from the *Bacillus* Genetic Stock Center. Spore preparation and purification was performed as described previously.[21,22] The liquid cultures were centrifugued at 6000 rpm for 15 min. They were washed twice with autoclaved MilliQ water at 6000 rpm for 15 min. The pellets were then resuspended in 5 mL of the same water and stored in the dark at room temperature. The pellets were allowed to sit in MilliQ water for a couple days so that any vegetative cell "contaminants" would autolyze and the debris would be washed away with the latter washes. Subsequently, the spore pellets were washed as described above an additional four times. The pellets were resuspended in 2 mL of the same sterile MilliQ water. One microliter of the *Bti* spore suspension was placed onto a clean 5 × 5 mm Si wafer and air-dried in a laminar flow hood. Prior to NanoSIMS analysis, samples were introduced into the vacuum chamber and evacuated to less than 1×10^{-5} Torr in ~5 min.

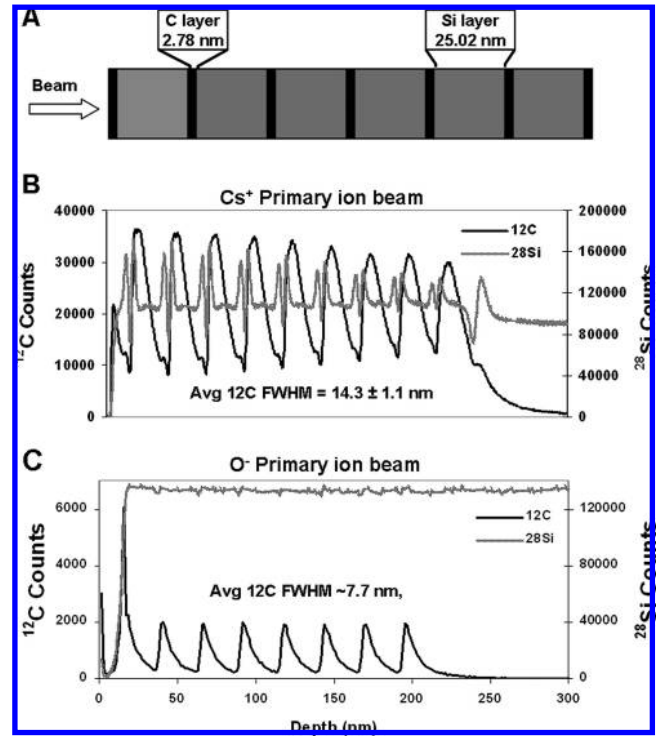

Figure 1. Depth profile analysis of a C−Si multilayer by NanoSIMS. (A) Model representation of the multilayer showing the alternating C and Si layers. C and Si elemental depth profiles acquired with (B) Cs[22] and (C) O^- primary ion beams.

For the lithium ion uptake experiment, 10 μL of the *Bti* spore suspension was added to 10 μL of 0.4 mM LiF solution in water for 15 min at room temperature. The LiF−spore mixture was vortexed to ensure uniform mixing. At the end of the exposure period, the suspension was washed four times consecutively by the following procedure. The suspension was centrifuged to isolate the spores from the solution followed by removal of the supernatant; the spores were then resuspended in water and the entire process repeated. Finally, 1 μL of the washed spore suspension in water was deposited onto a clean 5 × 5 mm Si wafer and air-dried in a laminar flow hood. Prepared samples were stored in dry boxes under argon. Prior to analysis, samples were introduced into the vacuum chamber and evacuated to less than 1×10^{-5} Torr in ~5 min.

(17) Wilson, R. G.; Stevie, F. A.; Magee, C. W. In Secondary Ion Mass Spectrometry: A practical handbook for depth profiling and bulk impurity analysis; John Wiley & Sons: New York, 1989.
(18) Gillen, G.; Fahey, A.; Wagner, M.; Mahoney, C. *Appl. Surf. Sci.* **2006**, *252*, 6537–6541.
(19) Cheng, J.; Wucher, A.; Winograd, N. *J. Phys. Chem. B: Condens. Matter Mater. Surf. Interfaces Biophys.* **2006**, *110*, 8329–8336.
(20) Plomp, M.; Leighton, T. J.; Wheeler, K. E.; Malkin, A. J. *Biophys. J.* **2005**, *88*, 603–608.
(21) Longchamp, P.; Leighton, T. J. *Lett. Appl. Microbiol.* **2000**, *31*, 242.
(22) Nicholson, W. L.; Setlow, P. In Molecular Biological Methods for Bacillus; John Wiley & Sons: West Sussex, UK, 1989.

Sectioned Spore. Spore samples were sectioned using a focused ion beam technique.[23] Sectioning exposed the spore interior, which was then characterized through 2-D analysis of the sectioned surface.

Secondary Ion Mass Spectrometry Analysis. SIMS was performed using the NanoSIMS 50 (Cameca Instruments, Geneviers, France) in simultaneous secondary ion collection mode with pulse counting on electron multipliers.[13] This enables simultaneous collection of five elements or isotopes originating from the same sputtered volume of a sample. A micro-cesium or a duoplasmatron source was used to generate Cs^+ or O^-/O_2^- primary ions, respectively, with 16 kV impact energy for sample interrogation. The primary beam was stepped across the sample to produce element-specific, quantitative digital images. The Cs^+ primary ion beam enhances the yield of electronegative elements and was used to analyze samples for C^-, F^-, Si^-, P^-, and Cl^- ions. The O^- primary ion beam, which enhances the yield of electropositive elements, was used to analyze samples for C^+, Li^+, Si^+, and Ca^+ ions. C and Si were analyzed in both modes. The lateral resolution of the secondary ion image is controlled by the primary beam spot size. For the detection of electronegative elements, a 1−6 pA Cs^+ primary beam was focused to a nominal spot size between 100−200 nm and stepped over the sample in a 256 × 256 pixel raster to generate secondary ions. For electropositive elements, a 10−100 pA O^- beam was used. In case of the O^- primary beam, the spot size was between 300 and 500 nm. Dwell time was 1 ms/pixel, and raster area was between 6 and 100 μm^2. The mass spectrometer was tuned for ~3000 mass resolving power to resolve isobaric interferences. NanoSIMS is an ultra-high-vacuum (UHV) technique so samples were evacuated to UHV conditions (1×10^{-10} Torr) prior to analysis. Spore samples were not coated with a conducting film or presputtered prior to analysis to minimize the introduction of analytical artifacts. The advantage of using a conductive coating is that it minimizes charging and nonequilibrium sputtering effects, such that the initial data are of better quality. However, for the spore samples charging was negligible in the absence of conductive coating.

Data were processed as quantitative elemental images using custom software (LIMAGE, L.R. Nittler) and were corrected for detector dead time and image shift during analysis. For quantification, the NanoSIMS secondary ion intensities were normalized to ^{12}C or ^{40}Ca to minimize systematic signal intensity variations that arose during the measurements. To minimize the complications of edge-related effects, only data from the central region of the spore was used for quantification purposes.

RESULTS AND DISCUSSION

Depth Profile Analysis of Silicon−Carbon Multilayer Sample. Typical depth resolution accessible in NanoSIMS measurements was estimated based on the analysis of a model silicon/carbon multilayer sample with alternating layers of C and Si of known dimensions: 2.78 nm for C and 25.02 nm for Si (Figure 1), Depth resolution is characterized by the increase in apparent interface thickness due to sputtering. Interface thickness can be defined as the depth interval over which the secondary ion intensity drops from 84 to 16% of the maximums. It can also be defined as the full width at half-maximum (fwhm) for layers that are significantly thinner than the depth resolution. Sputtering-induced mixing within the sample typically leads to gradual (vs abrupt) change in signal intensity across an interface.[17] Figure 1B shows the ^{12}C and ^{28}Si depth profiles acquired with the Cs^+ primary beam. The double Si peaks seen in the Si depth profile data are likely the result of a combination of factors; i.e., significant changes in ^{28}Si ion yield at the Si−C interfaces, differences in sputter rates for the Si and C layers, and the formation of an alloy between Si and C (SiC) through interdiffusion at the interface. It is evident from Figure 1B that the sputtering yield decreased with increasing depth while the fwhm value for carbon increased. These effects are likely due to the increase in mixing of the surface layer by the primary ion beam and increasing surface roughness with depth as a result of sputtering. The inverse relationship between sputtering yield and surface damage has previously been reported.[24] Depth resolution of the Cs^+ primary beam was determined to be 14.3 nm based on the average fwhm value of the carbon peak in depth profile data.

Figure 1C shows depth profile data acquired with the O^- primary beam. In this case, the ^{28}Si depth profile was not well resolved. The depth resolution was determined to be 7.7 nm based on fwhm value of the ^{12}C peak. The depth profiles of the Si−C multilayer structure were also processed using custom software (Replot PXT, Evans Analytical Group), which takes into account the nature of sputtering and ion yield effects in multicomponent materials. The depth resolution determined using the processed ^{12}C peak based on 84 to 16% definition was ~3 nm for the front interface and ~10.5 nm for the rear interface, with both O^- and Cs^+ primary beams. The lower depth resolution measured for the rear interface is caused by sputtering-induced perturbations in the interfacial region. In the case of spores, interface-induced artifacts are less likely due to the presence of a similar carbon based matrix throughout the spore.

While the multilayer sample is not directly comparable to the spore in morphology or composition, its purpose here has been to provide a well-characterized reference system for determining the potential depth resolution accessible with the current method. A unique feature of the NanoSIMS configuration compared to other SIMS instruments is that the primary ion beam is at normal incidence to the sample surface. Therefore, it is important to explicitly measure the depth resolution possible with this method for direct comparison with what is accessible by the other SIMS capabilities. Furthermore, the multilayer sample is composed of alternating carbon layers, and ion implantation into these layers may be comparable to biological samples such as spores.

Elemental Characterization of an Individual *Bti* Spore: Sectioned versus Whole Spore. Characterization of elemental distribution within a single spore has been reported previously for sectioned spores. Hence, for the purpose of comparison we report here spore elemental distribution information acquired by NanoSIMs based on (A) surface analysis of a sectioned spore and (B) depth profile analysis of a whole spore. Figure 2 shows the electronegative elemental profiles of *Bti* spore acquired with the Cs^+ primary ion beam for a sectioned and a whole spore. Comparison between the two profiles helps to demonstrate that both approaches, using sectioned or whole spores, provide

(23) Weber, P. K.; et al. Lawrence Livermore National Laboratory, unpublished work, 2007.

(24) Smentkowski, V. S. *Prog. Surf. Sci.* **2000**, *64*, 1–58.

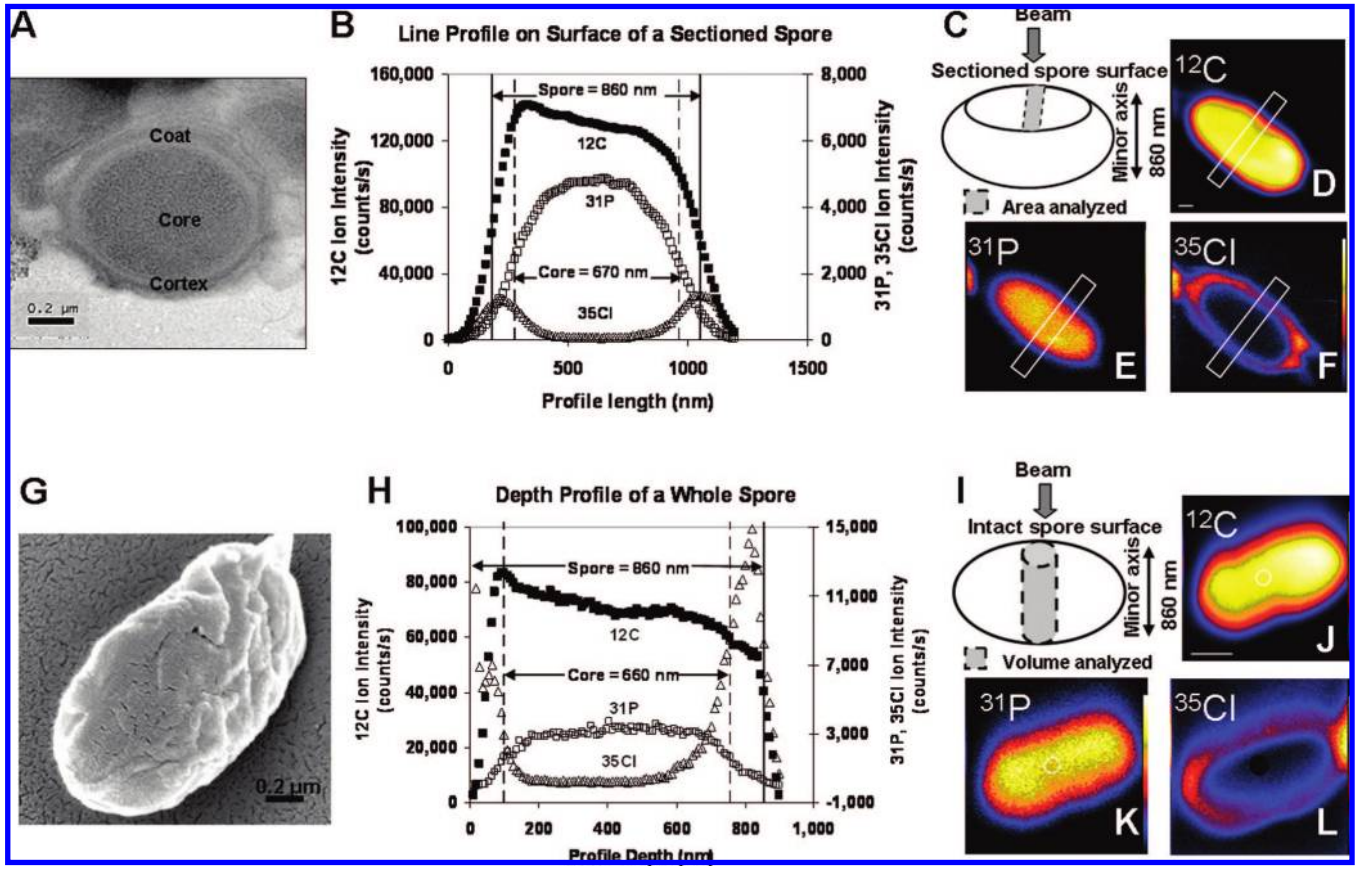

Figure 2. Comparison of NanoSIMS-based characterization of sectioned versus whole *Bti* spores. (A) TEM image of a sectioned *Bti* spore showing its layered architecture and overall dimensions. Scale bar 200 nm. (B) Lateral profile across the surface of a sectioned *Bti* spore showing the distribution of ^{12}C, ^{31}P, and ^{35}Cl. The dashed lines identify the core region based on the ^{31}P profile. The whole spore is defined based on the ^{12}C profile and identified by solid lines. Profile: length 1200 nm; width 200 nm. (C) Model representation of a sectioned spore with the highlighted rectangular region representing the location of profile data. (D−F) NanoSIMS secondary ion images showing the distribution of ^{12}C, ^{31}P, and ^{35}Cl across the sectioned spore surface. Scale bar 200 nm. (G) SEM image of a whole *Bti* spore. Scale bar 200 nm. (H) Depth profile of whole spore showing the distribution of ^{12}C, ^{31}P, and ^{35}Cl as a function of depth in the spore. (I) Model representation of a whole spore with the highlighted column representing the location of the profile data. Profile diameter 200 nm. (J−L) NanoSIMS secondary ion images showing the spatial distribution of ^{12}C, ^{31}P, and ^{35}Cl in the spore. Scale bar 500 nm. Both profiles were acquired with the Cs^{22} primary ion beam.

equivalent information on spore elemental distribution. However, depth profile analysis of whole spores requires minimal sample preparation and handling, compared to sectioned spores. It is worth noting that all spore elemental distribution information reported here represents data acquired from intact spores. Significantly damaged spores are characterized by the loss of P, Ca, and spore mass and therefore can be readily identified in NanoSIMS analysis based on these signatures (Supporting Information, Figure S1).

Surface data for the sectioned spore shown in Figure 2B represents a rectangular region 200 nm wide, with length plotted along the *x*-axis equal to 1200 nm. Each point on the profile represents the summed secondary ion data over a 200-nm line (along the width of the rectangular profile). Depth profile data shown in Figure 2H, acquired from a whole spore, represents a centrally located columnar region 200 nm in diameter, with height of the column representing the total sputtered depth. Each point on the depth profile graph represents the summed secondary ion data over a circular region 200 nm in diameter. A central location for the column is chosen in order to avoid edge-related sputtering artifacts. Given the radial symmetry of spores, the measured elemental distribution within the column is representative of the 3D elemental distribution for the whole spore.

Organic carbon content of the spore enabled it to be differentiated from the underlying Si substrate based on the carbon (^{12}C) secondary ion signal. The top hat structure of ^{31}P and ^{12}C depth profiles acquired with Cs^+ primary beam outlines the core region and the spore as a whole, respectively, and thus is representative of the spore structure. In these measurements, dimension of the spore minor axis is equivalent to the fwhm of the lateral ^{12}C ion profile (Figure 3). The value of the spore minor axis obtained by this method is in good agreement with the value determined by atomic force microscopy.[20] In measurements with the Cs^+ primary beam, the spore core is defined by the ^{31}P secondary ion signal. For both sample presentations, sectioned versus whole spore, the high ^{31}P ion signal, representing the core, is centrally localized within the spore, the spore outline being defined by the ^{12}C ion profile (Figure 2B and H). Unlike ^{31}P, chlorine (^{35}Cl) which is present as a trace element in spores, has higher abundance at the spore coat/cortex region, relative to the core. This is evident from relative positions of the two maximums in ^{35}Cl profile. The

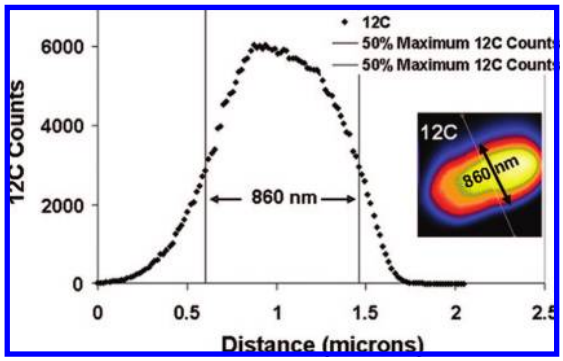

Figure 3. Lateral profile showing the ^{12}C distribution across the spore surface (inset). The inset shows a total ^{12}C ion spore image with the line representing the profile data. The vertical lines in the plot identify the two opposite edges of the spore and are based on 50% of maximum ^{12}C intensity.

high chlorine content of the coat/cortex region is likely due to the presence of KCl in the sporulation media.

Characterization of Lithium Distribution in *Bti* Spores Exposed to LiF Solution. In order to investigate the impact of environmental exposure on spore elemental distribution, we exposed *Bti* spores to aqueous LiF solution and then characterized the resultant elemental distribution in spores by depth profile analysis. The choice of lithium was based on the observation that *Bti* spores have extremely low abundance of endogenous Li (this was verified experimentally), and therefore, Li uptake by the spore is readily identifiable. Exposure to LiF solution resulted in the uptake and distribution of Li throughout the entire spore, thereby demonstrating that environmental exposures can alter the spore elemental distribution significantly. This supports the applicability elemental distribution and abundance in spores as a potential forensic tool.

Li is detected as an electropositive secondary ion; therefore, depth profile analyses were performed with the O^- primary ion beam. Spore-related elemental depth profiles (specifically ^{12}C and ^{40}Ca) acquired with the O^- primary beam (Figure 4) do not possess the top hat structure seen for spore elemental depth profiles (^{12}C and ^{31}P) acquired by the Cs^+ primary beam. However, the relative distributions of the different elements (C, Ca, Li, and Si) acquired with O^- primary beam are self-consistent and agree with previously established spore elemental composition.[9] For instance, since Ca is strongly associated with the core, the margin of the core in the depth profile is identified based on the distribution of Ca/C ion ratio. Figure 4A shows O^- primary beam acquired elemental depth profiles averaged over multiple spores. The average elemental distribution is in good agreement with the distributions measured in an individual spore (Figure 4B). Preferential uptake of metal cations by bacterial surfaces is a well-known phenomenon.[25] Based on this knowledge, it is expected that the highest content of Li in the spore exposed to LiF will be at the coat/cortex region. This is in general agreement with the presence of two peaks toward the beginning and end of the spore ^7Li depth profile data. Detailed discussion of the criteria used in determining boundaries of the spore core and coat/cortex regions based on the elemental depth profiles is given below in the section on spore sputter rate calculation.

(25) Doyle, R. J.; Matthews, T. H.; Streips, U. N. *J. Bacteriol.* **1980**, *143*, 471–480.

Elemental depth profiles of the spore acquired with the O^- primary beam lack the symmetric structure evident in the Cs^+ primary beam-acquired depth profiles and also appear to be somewhat dependent on the actual element. The asymmetric structure of ^{12}C and ^{40}Ca depth profiles is indicative of the loss in sputtering yields of these elements with depth. Similar behavior is observed with the sputtering of ^{12}C and ^{40}Ca in a calcite sample. In contrast, the symmetric structure of the ^7Li depth profile acquired simultaneously does not show the same loss in sputtering yield with depth and is more representative of the expected Li distribution in the spore. Sputtering-induced surface damage has been shown to increase with depth and leads to the lowering of sputtering yield.[23] In the case of the calcite sample, we have observed the sputter-induced increase in sample roughness with depth (Supporting Information, Figure S2). The fact that the spore Li depth profile is significantly different from the ^{12}C and ^{40}Ca profiles suggests that in the case of Li the effect of surface roughening on the sputtering yield is offset by some other factor, such as the migration of Li ion to the O^- charged surface. Given the greater diffusivity of the Li ion, this is a reasonable explanation.[26] However, further studies are needed to verify this hypothesis.

Calculation of Sputter Rate. In depth profile analysis, the depth scale is determined by the sputter rate. Sputter rate is used to convert the measured sputter time into depth and thereby extract depth-resolved compositional information about the sample. The sputter rate for a sample is determined based on the time required to sputter a known or measured depth of the sample using known primary beam current for a given raster area. The sputter rates reported here have been calculated using eq 1 and have units of (nanometer·micrometer^2)/(picoampere·second).

$$\text{sputter rate} = \frac{\text{sputtered depth} \times \text{raster area}}{\text{primary beam current} \times \text{sputter time}} \quad (1)$$

Sputter Rate in *Bti* Spore with Cs^+ Primary Beam. In depth profile analysis of whole spores, the sputtered depth at which the ^{12}C signal intensity decreases to 50% of its maximum value, is equivalent to the dimension of the spore minor axis. Dimension of the spore minor axis is determined from the ^{12}C ion line profile and is equivalent to the fwhm (Figure 3). This measurement gives an experimentally determined value of ~860 nm for the spore minor axis, which is in excellent agreement with the value of 872 ± 47 nm based on atomic force microscopy measurements.[20] In a similar manner, the dimension of the core minor axis is determined based on the ^{31}P ion profile. This gives a measured value of ~670 nm for the core width, which is in good agreement with a value of ~600 nm based on electron microscopy measurement of sectioned *Bti* spore.[10] Sputter rate for the spore is determined using eq 1, based on the time required to sputter the whole spore (sputtered depth being equivalent to the spore minor axis). Experimentally determined average sputter rate for *Bti* spore with the Cs^+ primary beam is 2.5 nm·μm^2/pA·s (Supporting Information). We also calculated separate sputter rates for the core and the coat/cortex regions of the spore. Both the regions have similar sputter rates given similar analytical conditions. The estimated thicknesses of 100 and 670 nm for the coat/cortex and core

(26) Giletti, B. J.; Shanahan, T. M. *Chem. Geol.* **1997**, *139*, 3–20.

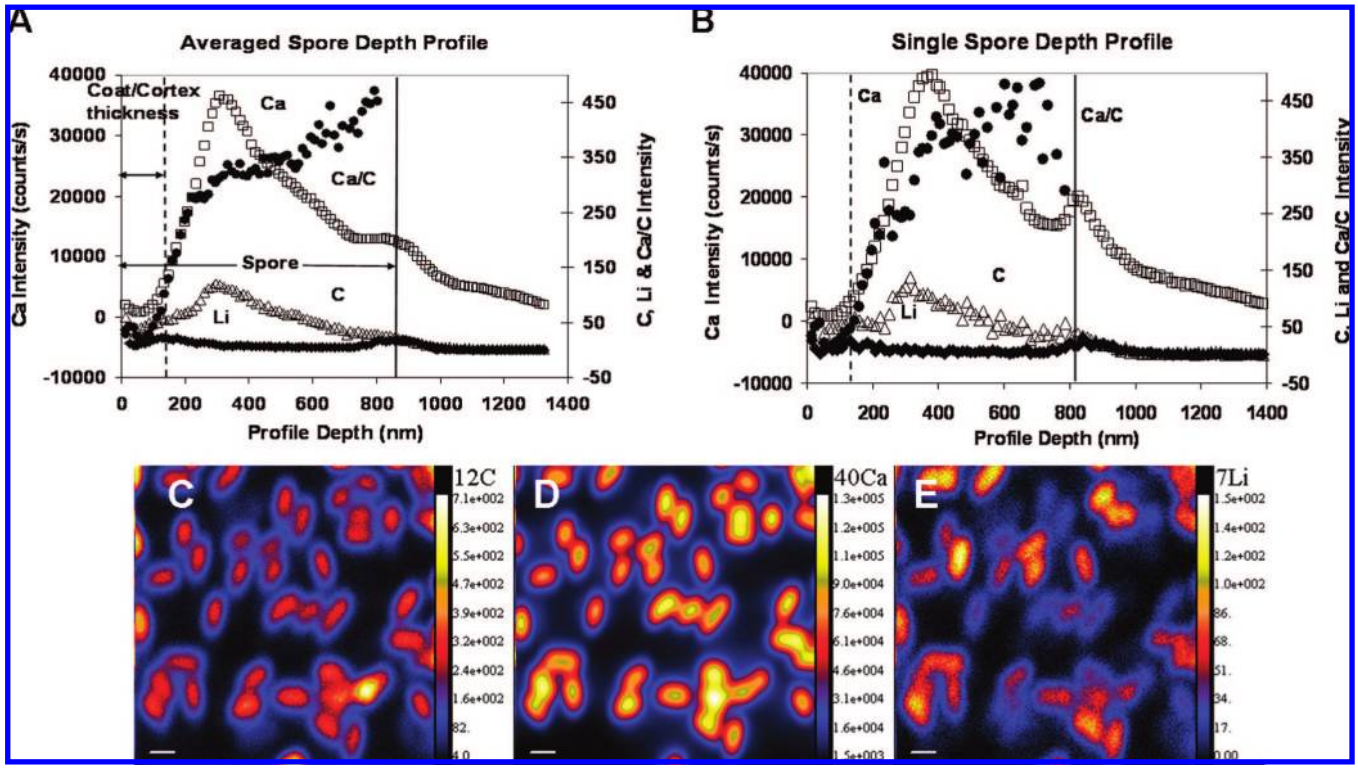

Figure 4. NanoSIMS-based depth profile of whole *Bti* spores acquired with the O^- primary ion beam. ^{12}C (△), ^{40}Ca (□), ^{7}Li (◆), and $^{40}Ca/^{12}C$ (ion/ion) ratio (●) distributions as a function of sputtered depth. (A) Averaged depth profiles for 12 spores, representative core (496 nm) and edge (856 nm) values of average elemental distribution in spores are as follows: ^{12}C, 71.8 ± 4.0 (core), 22.8 ± 1.9 (edge); ^{40}Ca, 23504 ± 858 (core), 12616 ± 687 (edge); ^{7}Li, 6.1 ± 1.7 (core), 18.0 ± 5.2 (edge). (B) Distributions measured in a single spore. The dashed line in (A) defines the coat/cortex thickness based on the $^{40}Ca/^{12}C$ ion ratio (●). The solid line identifies the spore margin based on the ^{7}Li (◆) profile. (C−E) NanoSIMS secondary ion images showing the distribution of ^{12}C, ^{40}Ca, and ^{7}Li in whole spores. Scale bar 1 μm.

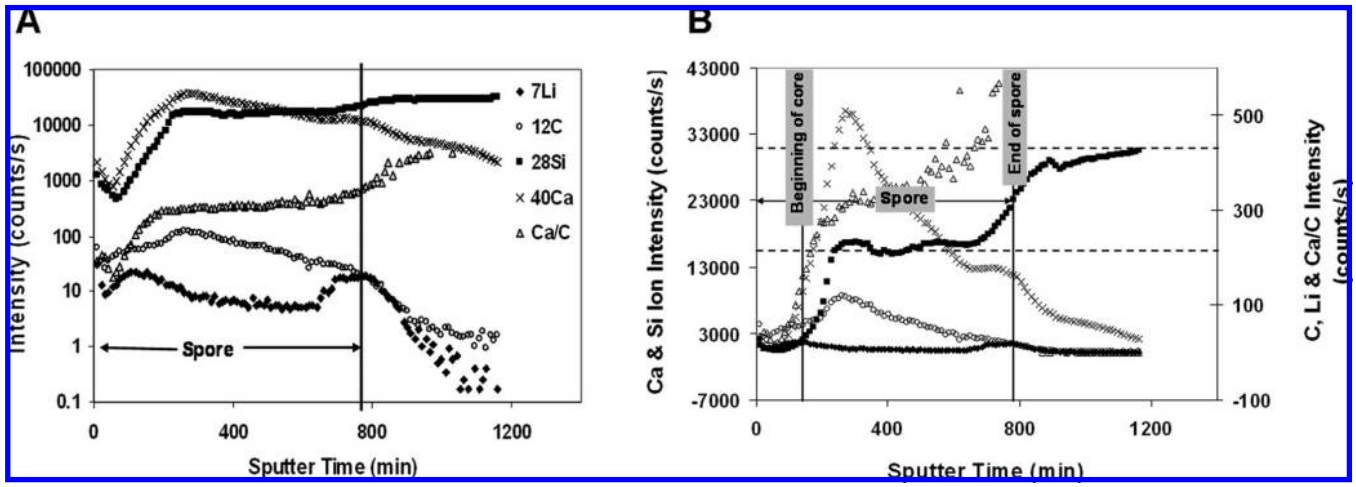

Figure 5. Depth profile analysis of a single spore with the O^- primary ion beam showing the distribution of ^{12}C (○), ^{40}Ca (×), ^{7}Li (◆), ^{28}Si (■), and Ca/C ion ratio (△) (A) logarithmic scale and (B) linear scale for the *y*-axis within the spore as a function of the sputter time. The spore body and the core region are identified based on elemental and ion ratio distributions.

regions, respectively, based on the sputter rate, agree well with the expected values.[10] Figure 2A shows electron microscopy (TEM) analysis of a sectioned *Bti* spore with three distinct regions: coat, cortex, and core. The general agreement between spore dimensions determined from NanoSIMS-based depth profile analysis of whole spores and TEM measurements of sectioned spores validates our sputter rate estimations.

Sputter Rate in *Bti* Spore with O^- Primary Beam. Calculation of sputter rate in spores with the O^- primary beam is complicated by the asymmetric structure of the ^{12}C and ^{40}Ca depth profiles. To overcome this limitation, we used ^{28}Si and ^{7}Li depth profile data in conjunction with Ca/C ion ratio data to determine the spore structure (Figure 5). The rationale behind this approach is the fact that spores are dispersed on Si wafers. In depth profile analysis of spores dispersed on Si wafers, one would expect the Si signal to approach its maximum intensity once the entire spore volume has been sputtered away. The significant Si intensity observed throughout the sputtering process for the spore depth

profile shown in Figure 5 is likely the combined effect of the larger O^- primary beam diameter (~400 nm at the 2σ level) and the surrounding Si substrate. Si depth profiles of spores dispersed on non-Si substrates do not show the same high Si intensity throughout the spore.[27] In the Si depth profile, the interface between the spore surface and the silicon substrate is represented by the point where the Si signal intensity is halfway in value between the two plateau regions (Figure 5). This depth is equivalent to the spore minor axis in magnitude. The magnitude of the spore minor axis is determined as described above in the case of the Cs^+ primary beam. Based on this approach, the average sputter rate for *Bti* spore with the O^- primary beam is determined to be 0.1 nm·μm^2/pA·s.

During the initial period of sputtering, the elemental depth profile data appear to be displaced with respect to the expected elemental distribution in the spore (Figures 4 and 5). For instance, Li content in the spore is expected to be higher at the coat/cortex region relative to the core. However, in the frontal portion of the Li depth profile data, the maximum is located ~150 nm from the spore surface, which corresponds to a displacement of ~100 nm from its expected position. It is likely that this displacement is a function of the time required to reach sputtering equilibrium,and as discussed below other processes may be involved as well. The Ca/C ion ratio profile instead of the ^{40}Ca ion profile is proposed to identify the beginning of the core region in order to normalize for changes in the ^{40}Ca ion intensity related to sputtering-induced effects. The beginning of the core region (hence, the thickness of the coat/cortex region) is then determined based on the depth at which the Ca/C ion ratio is 50% of its plateau value. However, the average coat/cortex thickness determined by this method is 170 ± 10 nm, which is greater than the expected value of ~80 nm based on previous measurements.[10] This apparent discrepancy is likely due to changes in the ^{12}C ion intensity with depth, which indicates that the sputtering process is not in equilibrium. The sputtering process is typically expected to reach equilibrium with respect to O^- implantation, by a depth of 100 nm. However, it is possible that the following factors result in nonequilibrium sputtering conditions: (a) size of the primary ion beam relative to the spore, (b) sputtering induced change in the spore surface, or (c) change in the sputtering rate upon entering the core. Further investigations are necessary to understand the observed effects.

In the basal portion of the depth profile, structural information based on ^{12}C and ^{40}Ca ion intensities is effectively lost due to sputtering-induced roughening of the sample. However, there is general agreement between the observed location of the Li peak and the location of the spore margin based on the Si depth profile (see above). In summary, while the O^- primary beam depth profile is more complex than the Cs^+ primary beam depth profile, descriptions of the spore structure based on ^{28}Si, Ca/C ratio, and ^{7}Li depth profiles are in reasonably good agreement. The results described here for the spore structure and associated elemental signatures have been observed in multiple spores and the results are consistent.

Quantification of Elemental Content in *Bti* Spores. In terms of quantitative composition, the spore as a whole consists of ~50% C and ~2.4% Ca by weight and the core is composed of ~4.5% Ca by weight.[28] In these experiments, the weight percent of Ca in the core was determined to be 4.40 ± 0.29% (1SE), based on measured Ca/C ion ratios in spores and a calcite standard (Supporting Information). We used the trace analytical capability of NanoSIMS to measure the uptake of Li^+ into the core of *Bti* spores exposed to aqueous Li^+ ions. A 15-min exposure resulted in a spore core Li^+ content of 0.0002 ± 0.00003% by weight based on the Li/Ca ion ratio.

CONCLUSION

We have presented an analytical method using high-resolution secondary ion mass spectrometry for imaging and 3D compositional characterization of intact, individual bacterial spores. The high sensitivity and spatial resolution possible with this methodology enables direct imaging and quantification of elemental distributions within complex micrometer-sized samples such as spores. The method requires minimal sample preparation and as such offers a new tool for bioforensic application. We have used this approach to probe the variability in spore elemental distribution for attribution purposes.[27] Also, the dynamics solvated ion permeability in *Bti* spores and the resulting distribution of the permeating ions within the spore has been investigated using this methodology.[29] Apart from its applicability as a bioforensic tool, the analytical method described here also has the potential for characterizing the spatially resolved composition of biological materials in general. Furthermore, the incorporation of isotopic labeling is likely to enable the in situ study of cellular biotransformations.

ACKNOWLEDGMENT

We thank S. Bajt for the silicon/carbon multilayer samples, C. Ramon for help with sample preparation, and D. Phinney for helpful discussions. L. Nittler (Carnegie Institute of Washington) developed the NanoSIMS data processing software. This work performed under the auspices of the U.S. Department of Energy by Lawrence Livermore National Laboratory under Contract DE-AC52-07NA27344 and supported by the LLNL Laboratory Directed Research and Development program, the Federal Bureau of Investigation, and the Department of Homeland Security.

SUPPORTING INFORMATION AVAILABLE

Additional information as noted in text. This material is available free of charge via the Internet at http://pubs.acs.org.

Received for review March 28, 2008. Accepted May 28, 2008.

AC8006279

(27) Weber, P. K.; et al. Lawrence Livermore National Laboratory, unpublished work, 2007.

(28) Marquis, R. E.; Bender, G. R. *J. Bacteriol.* **1985**, *161*, 789–791.

(29) Ghosal, S.; Leighton, T. J.; Wheeler, K. E.; Hutcheon, I. D.; Weber, P. K. Lawrence Livermore National Laboratory, unpublished work, 2007.